



This is a repository copy of *Investigation of ion irradiation induced damages in iron phosphate glasses: Role of electronic and nuclear losses in glass network modification.*

White Rose Research Online URL for this paper:  
<http://eprints.whiterose.ac.uk/169653/>

Version: Published Version

---

**Article:**

Dube, C.L., Stennett, M.C. [orcid.org/0000-0002-8363-9103](https://orcid.org/0000-0002-8363-9103), Akhmadaliev, S. et al. (1 more author) (2020) Investigation of ion irradiation induced damages in iron phosphate glasses: Role of electronic and nuclear losses in glass network modification. *Journal of Non-Crystalline Solids: X*, 8. 100055. ISSN 2590-1591

<https://doi.org/10.1016/j.nocx.2020.100055>

---

**Reuse**

This article is distributed under the terms of the Creative Commons Attribution (CC BY) licence. This licence allows you to distribute, remix, tweak, and build upon the work, even commercially, as long as you credit the authors for the original work. More information and the full terms of the licence here:  
<https://creativecommons.org/licenses/>

**Takedown**

If you consider content in White Rose Research Online to be in breach of UK law, please notify us by emailing [eprints@whiterose.ac.uk](mailto:eprints@whiterose.ac.uk) including the URL of the record and the reason for the withdrawal request.



[eprints@whiterose.ac.uk](mailto:eprints@whiterose.ac.uk)  
<https://eprints.whiterose.ac.uk/>



Contents lists available at ScienceDirect

## Journal of Non-Crystalline Solids: X

journal homepage: [www.journals.elsevier.com/journal-of-non-crystalline-solids-x](http://www.journals.elsevier.com/journal-of-non-crystalline-solids-x)

# Investigation of ion irradiation induced damages in iron phosphate glasses: Role of electronic and nuclear losses in glass network modification

Charu L. Dube<sup>a,b,\*</sup>, M.C. Stennett<sup>b</sup>, S. Akhmaliev<sup>c</sup>, N.C. Hyatt<sup>b</sup><sup>a</sup> School of Nano Sciences, Central University of Gujarat, Gandhinagar, India<sup>b</sup> Immobilisation Science Laboratory, Department of Materials Science and Engineering, University of Sheffield, Sheffield, United Kingdom<sup>c</sup> Institute of Ion Beam Physics and Materials Research, Helmholtz-Zentrum Dresden-Rossendorf, Bautzner Landstraße 400, Dresden D-01328, Germany

## ARTICLE INFO

## Keywords:

Iron phosphate glasses  
 Ion beam irradiation  
 Irradiation damage  
 X-ray absorption spectroscopic measurement  
 Hardness

## ABSTRACT

Ion irradiation was used as a surrogate approach to mimic radiation induced modification in iron phosphate glass network. To understand the synergetic effect of electronic and nuclear energy losses in glass network modification, ions at different energies were employed. The iron phosphate glasses were irradiated with Au ions at different ion energies between 750 keV and 20 MeV. The ion beam irradiated samples were characterised by employing different techniques. The Fe L<sub>2,3</sub>-edge X-ray absorption spectra of irradiated samples reveal reduction of Fe<sup>3+</sup> to Fe<sup>2+</sup>, induced by ion beam irradiation. X-ray diffraction and electron microscopy imaging confirm formation of crystalline Fe<sub>3</sub>(P<sub>2</sub>O<sub>7</sub>)<sub>2</sub>, Fe<sub>4</sub>(P<sub>2</sub>O<sub>7</sub>)<sub>3</sub>, Fe(PO)<sub>4</sub>, and Fe(PO<sub>3</sub>)<sub>3</sub> phases. The origin of these crystalline phases may be attributed to induced stress in irradiated samples. The observed decrease in hardness of irradiated samples was attributed to formation of non-bridging oxygen.

## 1. Introduction

High-level nuclear wastes (HLW) require vitrification in suitable matrix prior to permanent disposal [1]. Iron phosphate glasses (IPG) are considered as one potential matrix for vitrification of HLW and plutonium residues [2] [3]. The radiation stability of the immobilising matrix is a key concern in the long-term safety case for disposal of vitrified products. The incorporated actinides undergo alpha decay, and thereby produce energetic recoil nuclei and alpha-particles along with low intensity gamma rays [4]. Energetic recoil nuclei deposit their energy in the matrix through elastic ballistic collisions. The alpha-particles of energy nearly 5 MeV deposit their energy in the glass matrix by local excitation and ionization processes [5]. Localised electronic excitation above a threshold value provides a way to the permanent displacement of atoms, and leads to damage creation in glass network [6]. Radiation damage due to both nuclear and electronic stopping processes may be expected to affect the glass durability and its mechanical stability. Therefore, it is important to study radiation induced modification in the vitrifying matrix. Ion beam irradiation provides a convenient method to simulate and accelerate radiation damage in glasses and other materials [7–9]. During passage of ions through a solid, they deposit their energy through two interactions: (i) at low incident ion energy up to 100 keV, ions transfer their energy via elastic nuclear collisions/stopping (Sn), which is responsible for ballistic damage creation in solids, and (ii) at high energies, induce damage by inelastic electronic collisions/stopping [10].

Depolymerisation of the glass network in borosilicate glass samples exposed to Kr ions of energy 74 MeV and Xe ions of energy 92 MeV was previously observed [11]. Toulemonde et al. have reported structural modification in vitreous SiO<sub>2</sub> by Au (~0.3–15 MeV) ion irradiation and the observed modification is explained with help of unified thermal spike model in elastic nuclear and inelastic electronic stopping regime [12].

In the present study ion irradiation method is employed as surrogate approach to study effects of radiation damage on waste immobilising matrix. Efforts have also been made to understand the effects of damage on structural integrity of matrix. Ion energies are chosen in different regime to study the synergetic effect of electronic and nuclear stopping on glass network modification.

## 2. Experimental details

Iron phosphate glass of composition Fe<sub>0.8</sub>P<sub>1.2</sub>O<sub>4.2</sub> (i.e. 60 P<sub>2</sub>O<sub>5</sub>–40 Fe<sub>2</sub>O<sub>3</sub>) was synthesised using NH<sub>4</sub>H<sub>2</sub>PO<sub>4</sub> and Fe<sub>2</sub>O<sub>3</sub>. All the reagents were purchased from Sigma Aldrich, UK, and were of purity 99.9%. The reagent powders were taken in stoichiometric ratio and melted at 1150 °C for 4 h in recrystallized alumina crucibles in a muffle furnace. The molten glass was cast into a steel mold and annealed at 500 °C for 1 h. Our processing parameters were guided by previous studies which successfully fabricated iron phosphate glasses under such conditions, with negligible volatilisation of P<sub>2</sub>O<sub>5</sub> [13]. <sup>57</sup>Fe Mossbauer spectroscopy analysis of the as produced glass,

\* Corresponding author at: School of Nano Sciences, Central University of Gujarat, Gandhinagar, India.

E-mail address: [charulata.dube@cug.ac.in](mailto:charulata.dube@cug.ac.in) (C.L. Dube).<https://doi.org/10.1016/j.nocx.2020.100055>

Received 3 July 2020; Received in revised form 13 August 2020; Accepted 8 September 2020

Available online 13 September 2020

2590-1591/ © 2020 The Authors. Published by Elsevier B.V. This is an open access article under the CC BY license

(http://creativecommons.org/licenses/by/4.0/).

**Table 1**  
Details of Gold ion irradiation parameters: energy and fluence.

Sample name	Ion type and energy	Fluence (ions/cm <sup>2</sup> )
IPG1	Pristine	Pristine
IPG2	750KeV	$2 \times 10^{14}$
IPG3	5 MeV s	$2 \times 10^{14}$
IPG4	10 MeV	$2 \times 10^{14}$
IPG5	20 MeV	$2 \times 10^{14}$

established the ratio  $Fe^{2+}/\Sigma Fe^{3+} = 0.15$ , typical of glasses produced under such conditions with similar composition [2]. The glass samples were cut into discs and subsequently polished. The polished samples ( $\sim 1 \mu m$  finish) were irradiated at Ion Beam facility located at HZDR Germany. The glass samples were irradiated with Au ions at different energy: 750 keV, 5 MeV, 10 MeV and 20 MeV. In order to study the role of electronic and nuclear losses in glass network modification, the ion energy range is chosen to cover the transition from the mainly nuclear stopping to nearly pure electronic stopping regime. The chosen fluence was  $2 \times 10^{14}$  ion/cm<sup>2</sup> to get representative damage of nearly 1 dpa. The fluence was kept constant for all energies. The sample classification and all the irradiation parameters are summarised in Table 1.

The ion energies for irradiation experiments were chosen to cover different loss regimes; (i) 750 keV Au ions having mainly nuclear loss (ii) 5–20 MeV Au ions having both nuclear and electronic losses. The electronic/nuclear losses of Au ions in the iron phosphate glass matrix at different ion energy and the displacement damage as function of ion penetration depth, obtained from SRIM/TRIM software are given in Figs. 1 and 2, respectively [14]. It can be seen from Fig. 1 that total deposited energy is nearly same at different Au ion energy. Fig. 2 shows the distribution of displacement damage as function of depth. Depending upon the ion energy, peak damage is located at different depth. The variation of total losses (deposited energy) with ion energy, obtained from SRIM calculation, is shown in Fig. 3.

The pristine and irradiated glass samples were characterised by using different techniques for structural and microstructural modifications in glass network. The Fe  $L_{2,3}$  X-ray absorption spectra for pristine and irradiated IPG samples were acquired in total electron yield mode on the Soft X-ray absorption spectroscopy (SXAS) Beamline 1 at the Indus 2 synchrotron, RRCAT, Indore. Data were acquired over the range 700–740 eV, covering the Fe  $L_{2,3}$  edge. X-ray diffraction patterns were acquired before and after ion irradiation in  $\theta$ - $2\theta$  geometry on a Bruker D2 phaser instrument with Ni filtered Cu K $\alpha$  radiation, equipped with a Lynxeye position sensitive detector (with discriminator settings optimised to reject Fe K $\alpha$  fluorescence). A

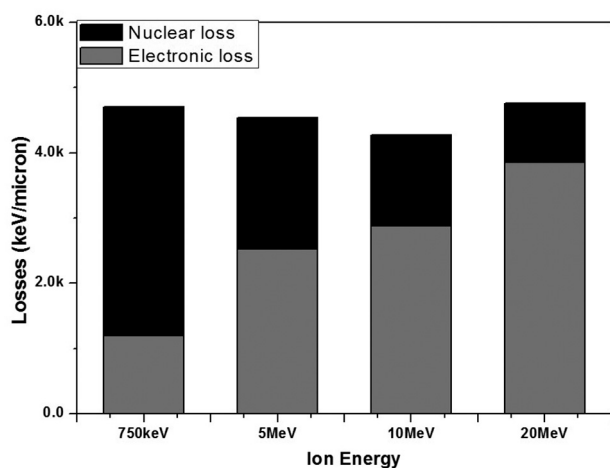


**Fig. 1.** Nuclear and electronic losses of gold ions deposited in IPG at different energy. (For interpretation of the references to colour in this figure legend, the reader is referred to the web version of this article.)

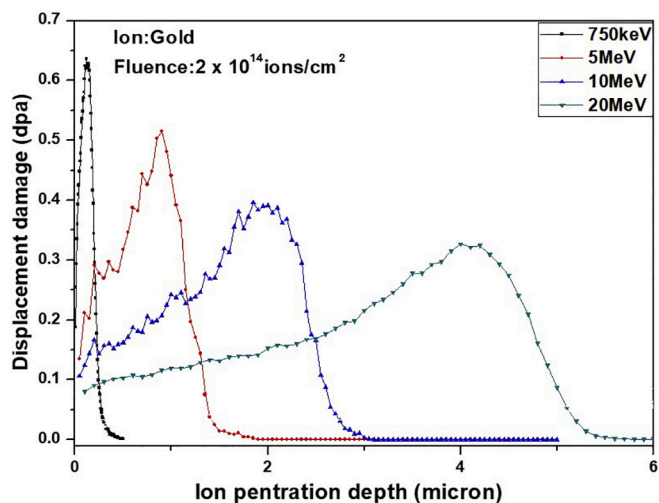


**Fig. 2.** The displacement damage versus ion penetration depth, for Au ions deposited in IPG.

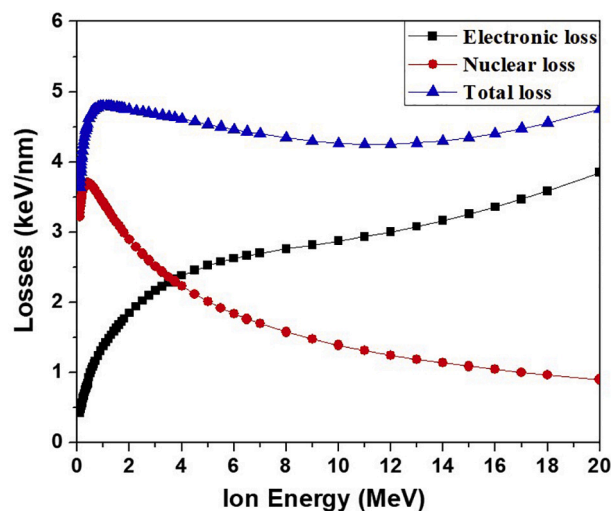


**Fig. 3.** Variation of total energy losses, and nuclear and electronic components, with ion energy.

Hitachi TM3030 SEM was utilised for imaging of the surface of the samples, prior to and following ion beam irradiation, with an accelerating voltage of 15 kV and working distance of  $\sim 8$  mm. Raman spectra in the range of  $800$ – $1500$   $cm^{-1}$  were collected on an inVia Raman microscope using laser light of wavelength 514.5 nm on pristine and irradiated glass samples. The acquired Raman spectra were deconvoluted to estimate irradiation induced modifications to the structure of the glasses. For nanoindentation measurements, sample was mounted on a stainless-steel stage. Measurements were carried out using Triboscope (Hysitron Inc.) nanoindenter with Berkovich indenter. Data were collected using automated  $4 \times 4$  matrix and data analysis was carried out using the procedure proposed by Oliver and Pharr [15].

### 3. Results and discussion

#### 3.1. X-ray absorption spectroscopic measurements:

To investigate the effect of radiation induced changes on iron speciation in glass matrix, Fe  $L_{2,3}$  edge X-ray absorption spectra of pristine and irradiated iron phosphate glass (IPG) samples were acquired in total electron yield mode. In total electron yield (TEY) mode, the probe depth is usually few nm ( $\sim 5$ – $10$  nm). Therefore, the ion beam induced

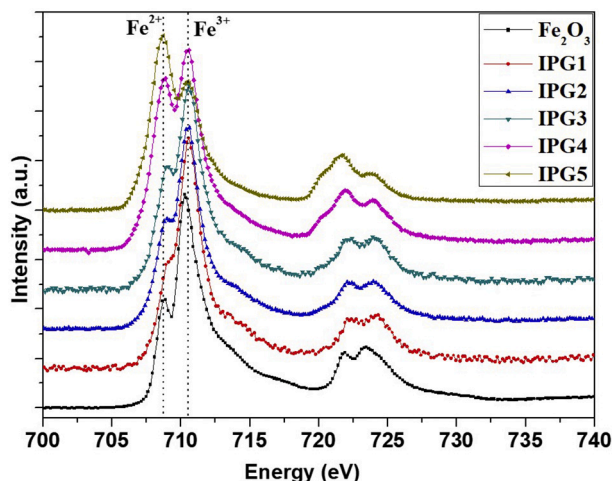


Fig. 4. Fe  $L_{2,3}$ -edge spectra for pristine and irradiated IPG samples.

Table 2

Deconvolution parameters for Raman spectra of pristine and irradiated IPG samples.

Sample name	Band centre ( $\text{cm}^{-1}$ )				Ratio of areas: $\nu_1/\Sigma\nu_{1-4}$
	Area under peak				
	$\nu_1$	$\nu_2$	$\nu_3$	$\nu_4$	
IPG6040_Pristine	952	1060	1125	1213	0.14
	25	98	27	24	
IPG6040_750keV	952	1060	1127	1218	0.15
	27	99	34	25	
IPG6040_5MeV	963	1060	1126	1217	0.16
	32	86	47	32	
IPG6040_10MeV	952	1060	1127	1224	0.17
	36	90	53	31	
IPG6040_20MeV	970	1062	1131	1220	0.18
	36	77	54	38	

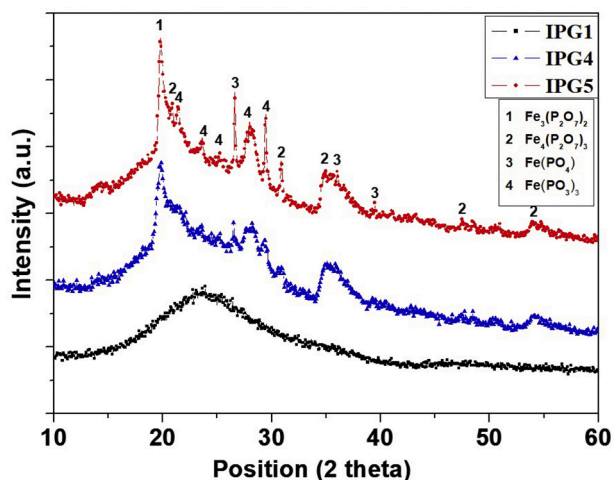


Fig. 5. X-ray diffraction patterns for pristine and irradiated IPG samples.

modifications, lying close to the sample surface will be probed. A  $\text{Fe}_2\text{O}_3$  sample as a reference was measured in parallel to IPG glass samples. The recorded spectra were calibrated to absorption maximum for the  $\text{Fe}_2\text{O}_3$  reference. The calibrated spectra were processed in Athena software for pre and post edge correction. The processed data are shown below in Fig. 4. The  $\text{Fe } L_3$  and  $L_2$  edges, located at  $\sim 710$  eV and 723 eV, are assigned to electronic transitions from  $\text{Fe } (2p)$  to hybridized  $\text{O}(2p)\text{-Fe}(3d)$  orbitals [16]. The local electronic structure of the

absorbing atom, such as its oxidation state and co-ordination environment, strongly affect the shape and position the  $L_3$  and  $L_2$  edges. For the  $\text{Fe}_2\text{O}_3$  reference compound, with Fe in distorted octahedral co-ordination, crystal field splitting results in clearly observable features attributed to  $t_{2g}$  ( $\sim 708.8$  eV) and  $e_g$  ( $\sim 710.3$  eV) states (Fig. 4) [17]. The profile of envelope of the  $\text{Fe } L_3$  and  $L_2$  edge, for the IPG samples, is evidently a convolution of contributions arising from  $\text{Fe}^{3+}$  and  $\text{Fe}^{2+}$  species, which is expected for iron phosphate glasses [18]. The maximum shift in iron  $L_3$  and  $L_2$  edges, following ion beam irradiation, was observed for the IPG sample irradiated with Au ions of energy 20 MeV, for which the  $L_3$  and  $L_2$  edge shift was  $\sim 0.3$  and  $0.6$  eV, respectively. The onset of the  $\text{Fe } L_3$  edge is clearly displaced to lower energy with increasing energy of Au ion irradiation and comprises two components which can be interpreted as arising from  $\text{Fe}^{2+}$  (centred at  $\sim 709$  eV) and  $\text{Fe}^{3+}$  species (centred at  $\sim 710$  eV), by comparison with reference data [19]. The ratio of the  $\text{Fe}^{2+}$  to  $\text{Fe}^{3+}$  component evidently increases with increasing energy of Au ion irradiation, demonstrating progressive reduction of  $\text{Fe}^{3+}$  to  $\text{Fe}^{2+}$ . Note that it is not possible to accurately quantify the  $\text{Fe}^{2+}/\text{Fe}^{3+}$  ratio due to the additional contribution of crystal field splitting from each species, although the trend is clear.

In our previous report, the observed splitting of the  $\text{Fe } L_3$  edge for iron phosphate glasses irradiated with Au ions of energy 750 keV at fluence of  $2 \times 10^{15}$  ion/ $\text{cm}^2$ , was attributed to the irradiation induced reduction of  $\text{Fe}^{3+}$  to  $\text{Fe}^{2+}$  [20]. Toulemonde et al. performed extensive study on structural modification of vitreous  $\text{SiO}_2$  by Au ion irradiation. In the study, the energies of Au ions were chosen in regime ( $\sim 0.3\text{--}15$  MeV), where both nuclear and electronic energy losses are significant [12]. The synergistic model (unified thermal spike mode) unifying the role of the elastic collision with the inelastic energy dissipation is suggested to understand evolution of the damage track radii in different (nuclear to the electronic) energy regime in vitreous  $\text{SiO}_2$ .

In the present study, ion energy is selected in such a way that the total deposited energy is nearly same at each ion energy. It is evident from Fig. 3 that the total deposited energy is has both nuclear and electronic loss components. Furthermore, it can also be seen from Fig. 3 that nuclear loss is  $\sim 1$  keV/nm ( $\sim 20\%$  of total loss) even at 20 MeV Au ion energy. Hence, the role of nuclear energy losses cannot be ignored while considering glass network modification due to irradiation. Therefore, the change in iron speciation in irradiated IPG samples can be attributed to synergetic effect of nuclear and electronic losses. The unified thermal spike model as suggested by Toulemonde et al. can be invoked to explain the change in iron speciation in irradiated IPG samples.

### 3.2. Raman spectroscopic measurements

The obtained Raman spectra for pristine and irradiated IPG samples are shown in Fig. 8. Deconvolution of the Raman spectra afforded the following assignment with reference to literature data [21]:  $\nu_1 \approx 950\text{--}970$   $\text{cm}^{-1}$ , ( $\text{PO}_4$ ) asymmetric stretch of  $\text{Q}^0$  species;  $\nu_2 \approx 1060$   $\text{cm}^{-1}$ , ( $\text{PO}_3$ ) symmetric stretch of  $\text{Q}^1$  species;  $\nu_3 \approx 1125\text{--}1131$   $\text{cm}^{-1}$ , ( $\text{PO}_2$ ) symmetric stretch of  $\text{Q}^2$  species;  $\nu_4 \approx 1213\text{--}1220$   $\text{cm}^{-1}$ , ( $\text{PO}_2$ ) asymmetric stretch of  $\text{Q}^2$  species. The area and frequency of each of the deconvoluted bands are reported in Table 2.

To understand the effect of ion beam irradiation on the network structure of the IPG glass, the ratio of band areas  $\nu_1/\Sigma\nu_{1-4}$  was determined. This ratio increases systematically with increasing Au ion energy, implying an increase in the proportion of  $\text{Q}^0$  species and hence depolymerisation of the glass, and an increase in the non-bridging oxygen concentration.

### 3.3. X-ray measurements and electron microscopic investigation

The X-ray diffraction (XRD) patterns were collected before and after ion irradiation in  $\theta\text{-}2\theta$  geometry. The XRD patterns for pristine and irradiated sample are shown in Fig. 5. Crystallisation is clearly observed in the irradiated samples. The reflections labelled as 1–4 in Fig. 5, are attributed to  $\text{Fe}_3(\text{P}_2\text{O}_7)_2$ ,  $\text{Fe}_4(\text{P}_2\text{O}_7)_3$ ,  $\text{Fe}(\text{PO})_4$ , and  $\text{Fe}(\text{PO}_3)_3$  phases,

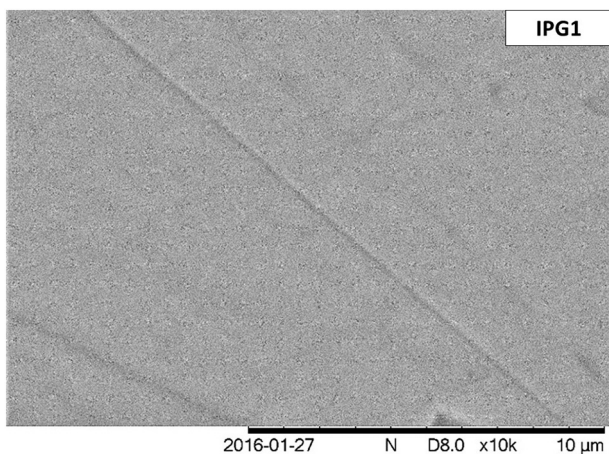


Fig. 6. Scanning electron micrograph of the surface of the pristine IPG sample.

respectively [22–24]. The most significant reflections identified in the XRD patterns correspond to  $\text{Fe}_3(\text{P}_2\text{O}_7)_2$  crystals. This is understandable also as  $\text{Fe}_3(\text{P}_2\text{O}_7)_2$  crystals have idealized structure of more disordered structure in an actual iron phosphate glass. Ion irradiation is non equilibrium process, having quenching rate of  $10^{12}$ – $10^{15}$  K/s, therefore possibility of spontaneous crystallisation is eliminated [24]. The energetic ions rapidly deposit energy along their path and it leads to huge temperature gradient between the ion path and its surrounding. Consequently, pressure wave gets induced in the wake of ion path and it develops a transient stress (greater than yield strength of the glass) as proposed by Jegadeesan et al. [24]. The developed transient stress leads to substantial deformation and hence shear band formation. The deformation may provide activation energy for nucleation of crystalline phases. Therefore, the observed crystallisation can be attributed to irradiation induced transient stress inside glass matrix, similar observation as discussed by Jegadeesan et al. [24].

The SEM images of the sample surface prior to and after irradiation are shown in Figs. 6 and 7. Crystal formation was observed in

microscopic images (Fig. 7) for samples irradiated at energies from 5 to 20 MeV. The crystallite size observed after irradiation at 5 and 10 MeV is  $\sim 50$  nm but ranges from 10 to 100 nm after irradiation at 20 MeV. The crystal formation may lead to dimensional changes and furthermore it can induce local stress causing some cracking inside the glass matrix [25]. Therefore, the formation of crystallites is detrimental for structural integrity of immobilisation matrix. In order to investigate irradiation induced effects on mechanical properties of glass matrix, hardness measurements have been carried out and results are discussed in next section.

### 3.4. Hardness measurements

Nanoindentation measurements were undertaken to determine the hardness values, the obtained hardness values are shown in Fig. 9. It can be seen from Fig. 9 that hardness is reduced for samples after ion beam irradiation. A 26% decrease in hardness values for IPG sample irradiated with 750 keV Au ions was observed. The increase in hardness with respect to plastic penetration depth for sample irradiated with 750 keV Au ions is attributed to shallow penetration of Au ions at energy of 750 keV (nearly 300 nm). The decrease in hardness for samples irradiated in energy regime 5–20 MeV is nearly the same and  $< 25\%$  of hardness value of pristine IPG sample. The decrease in hardness for samples irradiated at 5–20 MeV is reduced compared to the sample irradiated at 750 keV, this can be attributed to partial damage recovery due to electronic losses in IPG samples irradiated at 5–20 MeV [26]. This indicates that electronic energy loss did not have notable factor in hardness decrease, as reported by other groups as well [27]. The observed decrease in hardness can be explained by employing Sen's model [28]. The decrease in hardness values can be mainly attributed to increase in the concentration of non-bridging oxygen (NBO), as demonstrated by analysis of Raman spectra, which creates weak points in phosphate network [26]. Similar kind of decrease in hardness is reported by others as well in case of ion irradiated glass samples [28–30].

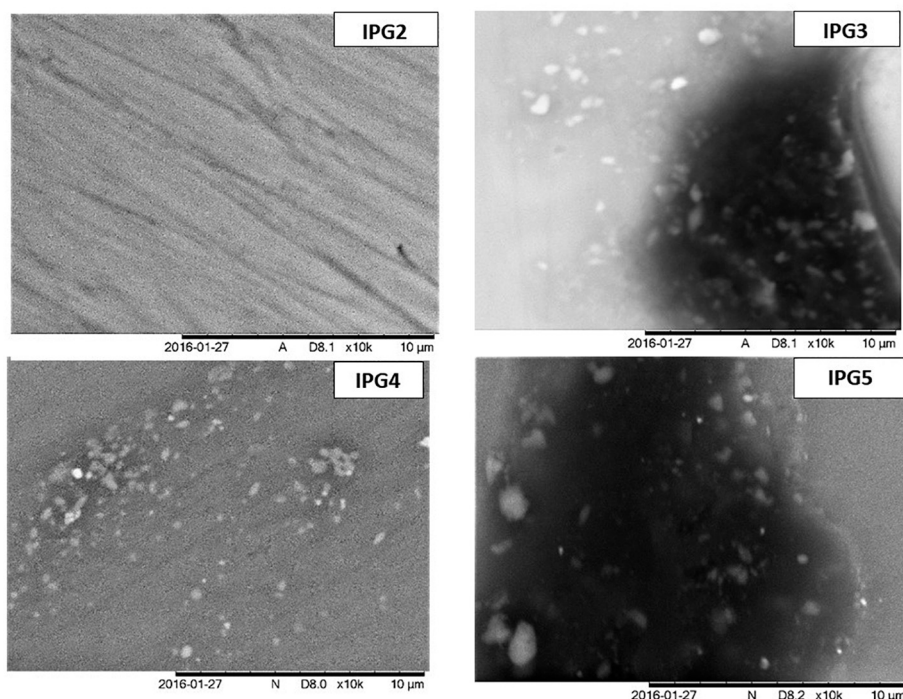


Fig. 7. Scanning electron micrograph of the surfaces of the irradiated IPG samples.

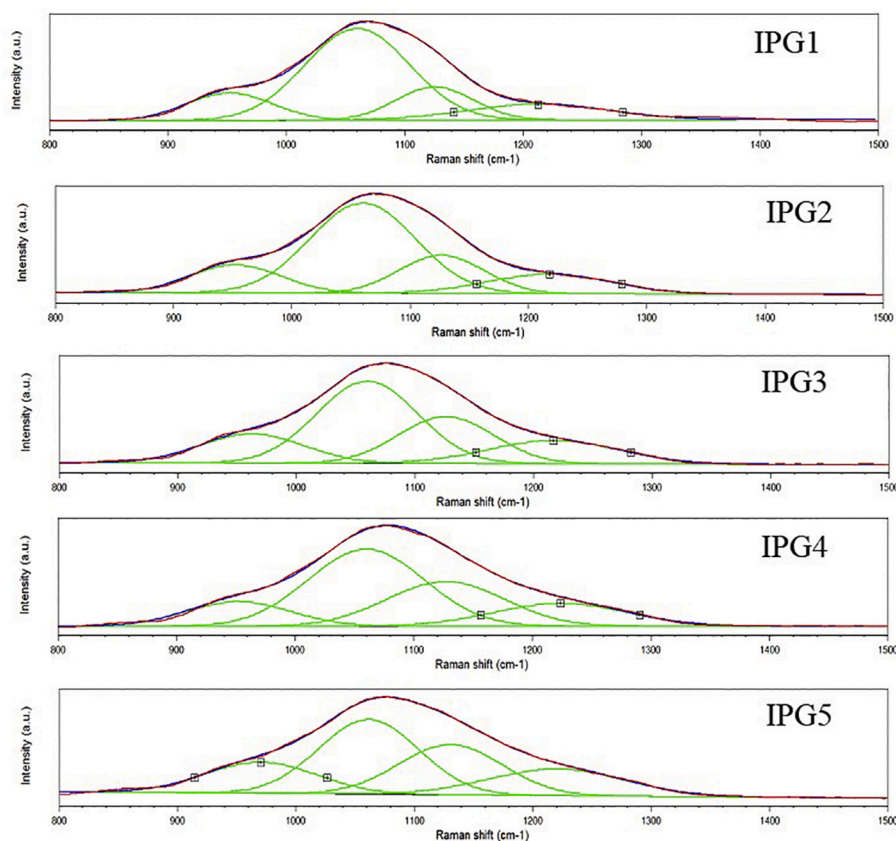


Fig. 8. Deconvoluted Raman spectra for the pristine and irradiated IPG samples.

#### 4. Conclusions

The irradiation experiments have been performed at the different Au ion energies. The iron 2,3-edge data shows insignificant iron reduction at Au ions energy of 750 keV. This can be attributed to small participation of electron losses and hence no iron reduction was observed. However significant iron reduction is observed in intermediate energy regime 5–20 MeV. The synergetic effect of nuclear and electronic losses is probably responsible for iron reduction in this regime. The X-ray diffraction results and electron microscopic images show formation of crystallites in energy regime of 5–20 MeV. The 26% decrease in hardness values for IPG sample irradiated with 750 keV Au ions is seen. The decrease in hardness values are nearly same (< 25%)

in energy regime of 5–20 MeV. It is anticipated that formation of crystallites and NBOs, as shown by Raman spectroscopy, are responsible for nearly similar decrease in hardness in this regime.

#### Credit author statement

**Charu L. Dube:** Conceptualization, Methodology, Data acquisition and curation, Writing- Original draft preparation.

**M. C. Stennett:** Sample preparation, Data curation, Reviewing.

**S. Akhmadaliev:** Performing ion irradiation experiments, Reviewing.

**N. C. Hyatt:** Supervision (Oversight and leadership responsibility for the research activity planning and execution), Project administration (Management and coordination responsibility for the research activity planning and execution) and acquisition of the financial support for the project leading to this publication.

#### Declaration of Competing Interest

The authors declare that they have no known competing financial interests or personal relationships that could have appeared to influence the work reported in this paper.

#### Acknowledgements

Authors are thankful to The Royal Academy of Engineering and Nuclear Decommissioning Authority for financial support. The work was supported by EPSRC (Grant references: EP/I012214/1, EP/K007882/1, and EP/M018792/1). Authors gratefully acknowledges help from Dr. Dinesh Shukla from Raja Ramanna Centre for Advanced Technology (Indus beamline 2), Indore, India for XAS measurements. This research was supported by the HADES/MIDAS facility at the

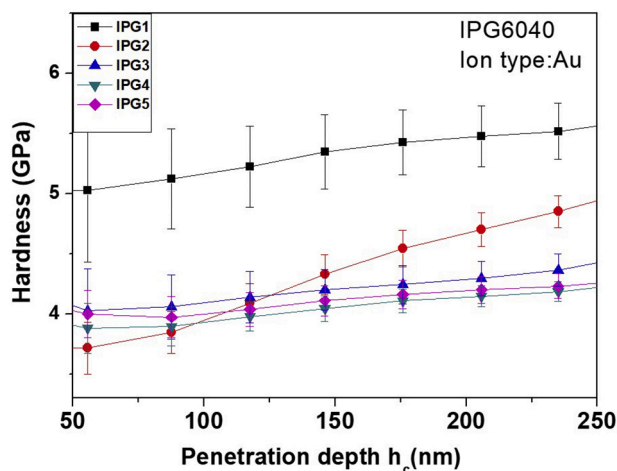


Fig. 9. Variation of hardness with depth.

University of Sheffield established with financial support from EPSRC and BEIS, under grant EP/T011424/1 [31].

## References

- [1] W.E. Lee, M.I. Ojovan, M.C. Stennett, N.C. Hyatt, Immobilisation of radioactive waste in glasses, glass composite materials and ceramics, *Adv. Appl. Ceram.* 105 (1) (2006) 3–12.
- [2] K. Joseph, M.C. Stennett, N.C. Hyatt, R. Asuvathraman, C.L. Dube, A.S. Gandy, ... R. Smith, Iron phosphate glasses: bulk properties and atomic scale structure, *J. Nucl. Mater.* 494 (2017) 342–353.
- [3] C.L. Dube, M.C. Stennett, A.S. Gandy, N.C. Hyatt, Simulation of alpha decay of actinides in iron phosphate glasses by ion irradiation, *Nucl. Instrum. Methods Phys. Res., Sect. B* 371 (2016) 424–428.
- [4] M.M. Bé, V. Chisté, C. Dulieu, E. Browne, V. Chechev, N. Kuzmenko, ... R. Dersch, Table of Radionuclides, (2004) (Vol. 2-A = 151 to 242) (Vol. 2).
- [5] G.W. Arnold, Ion implantation effects in alkali-borosilicate glasses, *Radiat. Eff.* 98 (1–4) (1986) 55–61.
- [6] J. De Bonfils, S. Peugeot, G. Panczer, D. De Ligny, S. Henry, P.Y. Noël, ... B. Champagnon, Effect of chemical composition on borosilicate glass behavior under irradiation, *J. Non-Cryst. Solids* 356 (6–8) (2010) 388–393.
- [7] A. Haddi, P. Trocellier, I. Draganic, F. Farges, S. Poissonnet, P. Bonnaillie, Ion irradiation behaviour and chemical durability of simple borosilicate glasses, *Nucl. Instrum. Methods Phys. Res., Sect. B* 266 (12–13) (2008) 3182–3185.
- [8] K.J. Yang, T.S. Wang, G.F. Zhang, H.B. Peng, L. Chen, L.M. Zhang, ... W. Yuan, Study of irradiation damage in borosilicate glass induced by He ions and electrons, *Nucl. Instrum. Methods Phys. Res., Sect. B* 307 (2013) 541–544.
- [9] H.H. Qarra, K.M. Knowles, M.E. Vickers, S. Akhmadaliev, K. Lambrinou, Heavy ion irradiation damage in Zr<sub>2</sub>AlC MAX phase, *J. Nucl. Mater.* 523 (2019) 1–9.
- [10] C.L. Dube, P.K. Kuliya, D. Dutta, P.K. Pujari, Y. Patil, M. Mehta, ... S.S. Khirwadkar, Positron annihilation lifetime measurement and X-ray analysis on 120 MeV Au + 7 irradiated polycrystalline tungsten, *J. Nucl. Mater.* 467 (2015) 406–412.
- [11] C. Mendoza, S. Peugeot, T. Charpentier, M. Moskura, R. Carballo, O. Bouty, ... C. Jegou, Oxide glass structure evolution under swift heavy ion irradiation, *Nucl. Instrum. Methods Phys. Res., Sect. B* 325 (2014) 54–65.
- [12] M. Toulemonde, W.J. Weber, G. Li, V. Shutthanandan, P. Kluth, T. Yang, ... Y. Zhang, Synergy of nuclear and electronic energy losses in ion-irradiation processes: the case of vitreous silicon dioxide, *Phys. Rev. B* 83 (5) (2011) 054106.
- [13] M.Z.H. Mayzan, M.C. Stennett, N.C. Hyatt, R.J. Hand, Graphite immobilisation in iron phosphate glass composite materials produced by microwave and conventional sintering routes, *J. Nucl. Mater.* 454 (1–3) (2014) 343–351.
- [14] J.F. Ziegler, J.P. Biersack, U. Littmark, *The Stopping and Range of Ions in Solids* New York, (1985).
- [15] W.C. Oliver, G.M. Pharr, An improved technique for determining hardness and elastic modulus using load and displacement sensing indentation experiments, *J. Mater. Res.* 7 (6) (1992) 1564–1583.
- [16] S. Shen, J. Zhou, C.L. Dong, Y. Hu, E.N. Tseng, P. Guo, ... S.S. Mao, Surface engineered doping of hematite nanorod arrays for improved photoelectrochemical water splitting, *Sci. Rep.* 4 (2014) 6627.
- [17] G. Cressey, C.M.B. Henderson, G. Van der Laan, Use of L-edge X-ray absorption spectroscopy to characterize multiple valence states of 3d transition metals; a new probe for mineralogical and geochemical research, *Phys. Chem. Miner.* 20 (2) (1993) 111–119.
- [18] C.S. Ray, X. Fang, M. Karabulut, G.K. Marasinghe, D.E. Day, Effect of melting temperature and time on iron valence and crystallization of iron phosphate glasses, *J. Non-Cryst. Solids* 249 (1) (1999) 1–16.
- [19] P.A. Van Aken, B. Liebscher, Quantification of ferrous/ferric ratios in minerals: new evaluation schemes of Fe L 23 electron energy-loss near-edge spectra, *Phys. Chem. Miner.* 29 (3) (2002) 188–200.
- [20] C.L. Dube, N.C. Hyatt, X-ray absorption spectroscopy in total electron yield mode: a powerful tool for surface characterization, in: D. Singh, S. Das, A. Materny (Eds.), *Advances in Spectroscopy: Molecules to Materials*, Springer, Singapore, 2019, pp. 133–139.
- [21] Y.M. Lai, X.F. Liang, S.Y. Yang, J.X. Wang, L.H. Cao, B. Dai, Raman and FTIR spectra of iron phosphate glasses containing cerium, *J. Mol. Struct.* 992 (1–3) (2011) 84–88.
- [22] K. Joseph, V. Yuvaraj, R. Govindaraj, A. Senapati, S. Ghosh, R.V. Krishnan, T.R. Ravindran, Iron phosphate glass from Fe<sub>4</sub>(P<sub>2</sub>O<sub>7</sub>)<sub>3</sub>: a new approach, *J. Non-Cryst. Solids* 520 (2019) 119327.
- [23] F. Wang, Q. Liao, K. Chen, S. Pan, M. Lu, Glass formation and FTIR spectra of CeO<sub>2</sub>-doped 36Fe<sub>2</sub>O<sub>3</sub>-10B<sub>2</sub>O<sub>3</sub>-54P<sub>2</sub>O<sub>5</sub> glasses, *J. Non-Cryst. Solids* 409 (2015) 76–82.
- [24] P. Jegadeesan, S. Amirthapandian, K. Joseph, C. David, B.K. Panigrahi, K.V.G. Kuty, Ion irradiation induced crystallization in iron phosphate glass—TEM investigations, *Adv. Mater. Lett.* 6 (2015) 224–227.
- [25] M.I. Ojovan, B.E. Burakov, W.E. Lee, Radiation-induced microcrystal shape change as a mechanism of wasteform degradation, *J. Nucl. Mater.* 501 (2018) 162–171.
- [26] A.H. Mir, I. Monnet, M. Toulemonde, S. Bouffard, C. Jegou, S. Peugeot, Mono and sequential ion irradiation induced damage formation and damage recovery in oxide glasses: stopping power dependence of the mechanical properties, *J. Nucl. Mater.* 469 (2016) 244–250.
- [27] M.L. Sun, H.B. Peng, B.H. Duan, F.F. Liu, X. Du, W. Yuan, ... T.S. Wang, Comparison of hardness variation of ion irradiated borosilicate glasses with different projected ranges, *Nucl. Instrum. Methods Phys. Res., Sect. B* 419 (2018) 8–13.
- [28] S. Sen, Z. Xu, J.F. Stebbins, Temperature dependent structural changes in borate, borosilicate and boroaluminate liquids: high-resolution <sup>11</sup>B, <sup>29</sup>Si and <sup>27</sup>Al NMR studies, *J. Non-Cryst. Solids* 226 (1–2) (1998) 29–40.
- [29] A.H. Mir, I. Monnet, B. Boizot, C. Jégou, S. Peugeot, Electron and electron-ion sequential irradiation of borosilicate glasses: impact of the pre-existing defects, *J. Nucl. Mater.* 489 (2017) 91–98.
- [30] P. Lv, L. Chen, B.T. Zhang, W. Yuan, B.H. Duan, Y.D. Guan, ... T.S. Wang, Composition-dependent mechanical property changes in Au-ion-irradiated borosilicate glasses, *J. Nucl. Mater.* 520 (2019) 218–225.
- [31] N.C. Hyatt, C.L. Corkhill, M.C. Stennett, R.J. Hand, L.J. Gardner, C.L. Thorpe, The HADES facility for high activity decommissioning engineering & science: part of the UK national nuclear user facility, *IOP Conf. Series* 818 (2020) 012022.